Improvement of Nonlinear Distortion in an IMPATT Stable Amplifier

HIDEMITSU KOMIZO, YOSHIMASA DAIDO, HIDEO ASHIDA, YUKIO ITO, AND MASAJI HONMA

Abstract—**More than a 40-dB third-order intermodulation product (IMP) has been achieved in a 13-GHz-band 2-stage IMPATT stable amplifier with 21-dBm output level and 11-dB gain, using a diode bias-current compensation technique.**

Theoretical calculations also verified the experimental data. This technique will enable the IMPATT stable amplifier to be used in a multicarrier AM transmission system.

I. Introduction

PRESENTLY, IMPATT diodes are widely used in microwave oscillators and amplifiers. Up-to-date frequency stabilizing techniques applied to IMPATT oscillators have been reported [1], [2] and the FM noise reduction technique was also treated in several papers [3], [4].

With these advanced technologies, these oscillators and amplifiers have been put into practical applications such as in FM [5] or PCM communication and radar systems. But, in applications to amplitude modulation systems, such as TV or SSB-AM transmission systems [6], the intermodulation products (IMP's) become an important practical factor. Several authors reported [7] in detail the measured IMP's produced in an X-band IMPATT stable amplifier. The third-order IMP's commonly observed at high-level operation in these IMPATT amplifiers are about 10~20 dB, which does not meet the required specifications for those AM systems. The nonlinear distortion produced in an IMPATT amplifier is an especially important problem still remaining to be overcome.

In this paper, a new technique to improve the IMP, produced in an IMPATT stable amplifier is described which utilizes a diode bias-current compensation according to the signal input level of the amplifier. Also described are a convenient method of measuring the dynamic admittance of the IMPATT diode and the theoretical calculations of the intermodulation products, to estimate the usefulness of this compensation technique.

A 13-GHz-band 2-stage IMPATT stable amplifier (with more than 21-dBm output level and 11-dB total gain) using this technique showed the third-order intermodulation product of more than 40 dB within the input level up to 10 dBm (the sum of two equal amplitude input signal levels). The improvement of the third IMP was as much as about 20 dB at the input level of 10 dBm. This has been qualitatively verified by theoretical calculations using the measured electronic admittance $\bar{y}_D$. This technique is essentially different from the feedforward scheme [8] in the following way—that the former compensates the distortion itself, but the latter cancels the distortion by adding the inverse phase distortion.

Manuscript received February 16, 1973; revised May 22, 1973.

H. Komizo, Y. Daido, H. Ashida, and Y. Ito are with the Radio Transmission Laboratory, Fujitsu Laboratories Ltd., Kawasaki, Japan.

M. Honma is with the Radio Engineering Department, Fujitsu Ltd., Kawasaki, Japan.

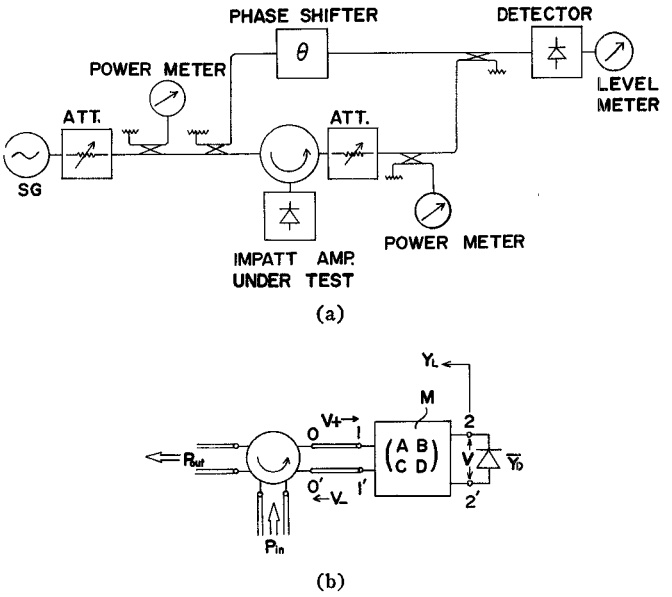

Fig. 1. (a) Measuring setup. (b) Amplifier circuit diagram.

Moreover, the latter scheme has more complicated circuits, including an additional RF amplifier. So the latter has more circuits loss than the former. This technique will enable IMPATT amplifiers to be used in various AM transmission systems.

II. Measurement of Electronic Admittance

A convenient way to measure the electronic admittance of a negative resistance device will be introduced in this section. Fig. 1(a) shows the measuring setup. The RF signal level dependency of two quantities is measured; one is the gain G_s and the other is the phase difference ϕ between incident wave V_+ of IMPATT amplifier and reflected wave V_-. The reference phase difference is measured by replacing the diode with a shorted one. The normalized electronic admittance can be derived from above-measured parameters. Fig. 1(b) shows the circuit diagram of a reflection-type amplifier. The network M in the figure is assumed to contain no loss. Therefore, the resultant electronic admittance contains some errors caused by this assumption. But this assumption causes little error in the output quantities such as IMP, distortion rate for the modulated signal, etc., which are calculated using this normalized electronic admittance and load admittance measured by the same manner. The fundamental parameters of the network M in Fig. 1(b) are denoted as A, B, C, and D. The relation between V_+ and V_- is easily derived using F-parameters of M, the electronic admittance $\bar{Y}_D$ of the IMPATT diode, and the characteristic impedance Z_0 of the transmission line be-

tween 1–1′ and 0–0′ in Fig. 1(b):

$$V_- = \frac{B - Z_0D(A - Z_0C)/(B - Z_0D) + \overline{Y}_D}{B + Z_0D(A + Z_0C)/(B + Z_0D) + \overline{Y}_D} V_+. \quad (1)$$

The load admittance Y_L looking to the left-hand side from 2–2′ is

$$Y_L = \frac{A + Z_0C}{B + Z_0D} \qquad Y_L{}^* = \frac{A - Z_0C}{DZ_0 - B} \quad (2)$$

where * means complex conjugate.

The assumption mentioned above is taken into account. For a lossless network, A and D are purely real, B and C are purely imaginary. Using (2), (1) is rewritten as

$$V_- = e^{-j\theta} \frac{Y_L{}^* - \overline{Y}_D}{Y_L + \overline{Y}_D} V_+ \quad (3)$$

where

$$e^{-j\theta} = \frac{Z_0D - B}{Z_0D + B}, \quad \left(\because \left| \frac{Z_0D - B}{Z_0D + B} \right| = 1 \right).$$

Then the reflection coefficient $\dot{\Gamma}$ is

$$\dot{\Gamma} = \Gamma e^{j\Psi} = e^{-j\theta} \frac{Y_L{}^* - \overline{Y}_D}{Y_L + \overline{Y}_D} \quad (4)$$

where Γ is the modulus of $\dot{\Gamma}$, and Ψ is the argument of $\dot{\Gamma}$. The relations between Γ, Ψ, and the measured parameters are as follows:

$$\Gamma = \sqrt{G_s}$$
$$-\Psi = \phi - \psi \quad (5)$$

where ψ is the unknown constant electric angle. When the diode is replaced by a shorted one, the relation between V_+ and V_- is

$$V_- = -e^{-j\theta} V_+ = e^{-j(\theta+\pi)} V_+.$$

Then

$$\theta + \pi = \phi_0 - \psi. \quad (6)$$

$\dot{\Gamma}$ is given by ϕ, ϕ_0, and G_s, using (5) and (6):

$$\dot{\Gamma} e^{j\theta} = \sqrt{G_s}\, e^{j(\phi_0 - \phi - \pi)} = -\sqrt{G_s}\, e^{j(\phi_0 - \phi)}. \quad (7)$$

The normalized electronic admittance $\bar{y}_D$ is defined as

$$\bar{y}_D = \frac{1}{G_L} (\overline{Y}_D + jB_L)$$
$$= \frac{1}{G_L} [-\overline{G}_D + j(\overline{B}_D + B_L)] \; (\equiv -\bar{g}_D + j\bar{b}_D) \quad (8)$$

where

$$Y_L = G_L + jB_L$$
$$\overline{Y}_D = -\overline{G}_D + j\overline{B}_D.$$

Using (4) and (7), $\bar{y}_D$ is given as follows:

$$\bar{y}_D = \frac{1 - G_s - j2\sqrt{G_s} \sin(\phi - \phi_0)}{1 + G_s - 2\sqrt{G_s} \cos(\phi - \phi_0)}. \quad (9)$$

Parameter $|u|$ is introduced which characterizes the RF amplitude of the IMPATT diode:

$$|u| = \sqrt{G_L}\, V_{RF} \quad (10)$$

where V_{RF} is the RF voltage applied to the diode. Generated power P_G from the diode is

$$P_G = (G_s - 1)P_{in} (= \tfrac{1}{2}\overline{G}_D V_{RF}{}^2 = \tfrac{1}{2}\bar{g}_D |u|^2) \quad (11)$$

where P_{in} is the input power of the RF signal. From (11), $|u|$ is determined as follows:

$$|u| = \sqrt{\frac{2(G_s - 1)P_{in}}{\bar{g}_D}}. \quad (12)$$

Then the normalized electronic admitance $\bar{y}_D$ is determined as the function of $|u|$; $|u|$ has the dimension of the square root of power. The results of this measurement are shown in Fig. 2(a) as a parameter of bias current. And $\bar{y}_D$ can be approximated with the power series of $|u|$ as follows:

$$\bar{g}_D = \overline{G}_D/G_L = g_0 - g_1|u| - g_2|u|^2$$
$$\bar{b}_D = (\overline{B}_D + B_L)/G_L = b_0 + b_1|u| + b_2|u|^2. \quad (13)$$

The bias-current dependency of the parameters $g_0 \sim b_2$ are shown in Fig. 2(b) and (c). The normalized load admittance locus can also be determined with similar measurement within the frequency range where the frequency dependency of the electronic admittance is negligible. The normalized load admittance y_L is defined as

$$y_L = \frac{1}{G_{L0}} (Y_L - jB_{L0}) \quad (14)$$

where G_{L0} and B_{L0} are the real and imaginary part of the load admittance used in the measurement of the normalized electronic admittance, respectively, and Y_L is the load admittance of another circuit condition.

III. Theoretical Calculation of Intermodulation Products

The IMP's of IMPATT stable amplifiers are produced by the RF voltage dependencies of the electronic admittance of IMPATT diodes. This process can be discussed using normalized electronic admittance $\bar{y}_D$, normalized load admittance y_L, and amplitude parameter $|u|$ defined in the previous section. The detailed mathematical treatments are as follows.

The equivalent circuit of the amplifier is shown in Fig. 3. The current source i corresponds to the input signal:

$$i = I_0(\cos \omega_1 t + \cos \omega_2 t) = 2I_0 \cos pt \cos \omega_0 t \quad (15)$$

where

$$\omega_0 = \frac{\omega_1 + \omega_2}{2} \qquad p = \frac{\omega_2 - \omega_1}{2}.$$

Input level varies with the angular frequency $2p(=\omega_2 - \omega_1)$, i.e., the period π/p. Then, the RF voltage amplitude of the active device changes with the fundamental period of π/p. Delay time exists between the variation of the input level and that of RF voltage amplitude. But, if p is much smaller than the operating bandwidth of the amplifier, the delay time is negligible. Then the amplitude of the RF voltage at the instant $t = t_0$ is calculated as the stationary value for the current

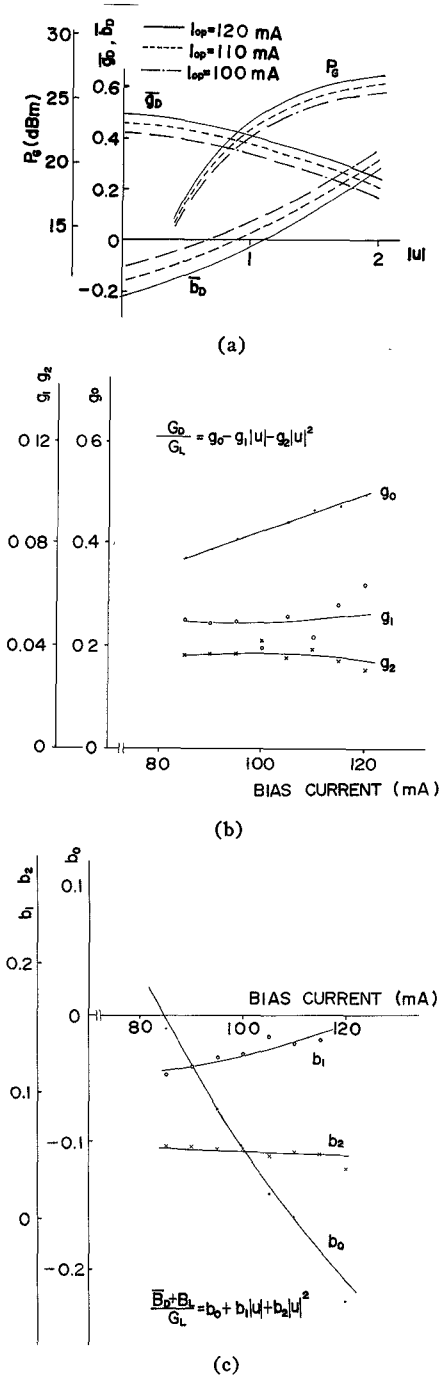

Fig. 2. (a) RF amplitude dependency of normalized electronic admittance and generated power as a parameter of bias current I_{0p}. (b) Bias-current dependency of electronic conductance. (c) Bias-current dependency of electronic susceptance.

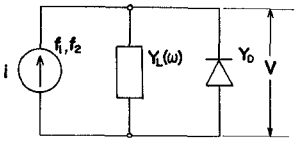

Fig. 3. Amplifier equivalent circuit.

source $2I_0 \cos pt_0 \cos \omega_0 t$. From the circuit equation, the following equation is derived:

$$4I_0^2 \cos^2 pt_0 = | Y_L(\omega_0) + \overline{Y}_D(V_{RF}) |^2 V_{RF}^2 \quad (16)$$

where V_{RF} is the RF voltage amplitude. From the definition of the normalized electronic admittance

$$| Y_L + \overline{Y}_D |^2 V_{RF}^2 = G_L | y_L + \bar{y}_D |^2 | u |^2$$

where y_L and $|u| = \sqrt{G_L}\, V_{RF}$ are defined in Section II. Then (16) becomes

$$(2I_0^2/G_L)(1 + \cos pt_0) = | y_L + \bar{y}_D(|u|) |^2 | u |^2. \quad (17)$$

The relation between I_0 and input power P_{in} is

$$I_0^2 = 4G_L P_{in}$$

where P_{in} is the sum of the powers of two spectrums. Then (17) becomes

$$8P_{in}(1 + \cos pt_0) = \{[g_L - \bar{g}_D(|u|)]^2 + [b_L + \bar{b}_D(|u|)]^2\} | u |^2. \quad (18)$$

And the voltage reflected wave V_- from the amplifier is given by

$$\sqrt{Y_0}\, V_- = 2\left(\frac{y_L^* - \bar{y}_D}{y_L + \bar{y}_D} \sqrt{P_{in}} \cos pt_0\right) e^{j(\omega_0 t + \theta)}, \qquad Y_0 = 1/Z_0 \quad (19)$$

where θ is the constant phase factor.

If the values of $|u|$ for various instant t_0 are calculated using (18), the values of $\sqrt{Y_0}\, V_-$ for various instant t_0 are given using (19). From these values of $\sqrt{Y_0}\, V_-$ the spectrums of $\sqrt{Y_0}\, V_-$ can easily be calculated. For each spectrum $\sqrt{Y_0}\, V_{-n}$ of $\sqrt{Y_0}\, V_-$, the output-power spectrum $(P_{out})_n$ is given by

$$(P_{out})_n = \tfrac{1}{2} | \sqrt{Y_0}\, V_{-n} |^2. \quad (20)$$

This calculation is applied to an amplifier and the results are compared with the measured one. The used amplifier has the following characteristics: the small-signal gain is about 8 dB with the bias current of 110 mA, the 1-dB compression input level is about 12 dBm, and the 1-dB bandwidth at 10-dBm input level is about 100 MHz.

In the measurement of the third- and fifth-order IMP's, two signals of f_1 and f_2 with equal amplitude were supplied to the amplifier. The frequency difference of both signals was set to 5 MHz. Fig. 4(a) shows both calculated and measured third- and fifth-order IMP's at the output port of the amplifier. IMP's are defined as the ratio of main carrier to the sidebands caused by the intermodulation. The calculated third-order IMP's are closely coincided with the measured one. In this case, normalized electronic admittance measured with this amplifier is used for the calculation of IMP's. This figure shows the validity of the measured normalized electronic admittance in a certain sense. The IMP's are dependent on both the gain and the carrier location to the center frequency of the amplifier. To evaluate the circuit dependency of IMP's, further calculations are carried out using the same normalized electronic admittance $\bar{y}_D$ and different normalized load admittance y_L. Normalized load admittance y_L on a certain circle in a rectangular complex admittance plane give the same gain for the input level corresponding to the circle. y_L is specified by determining the angular parameter Θ on the circle as shown in Fig. 4(b), together with the gain and the input level. IMP's are dependent on this parameter Θ. The dependencies of third-order IMP's are shown in Fig. 4(c) for

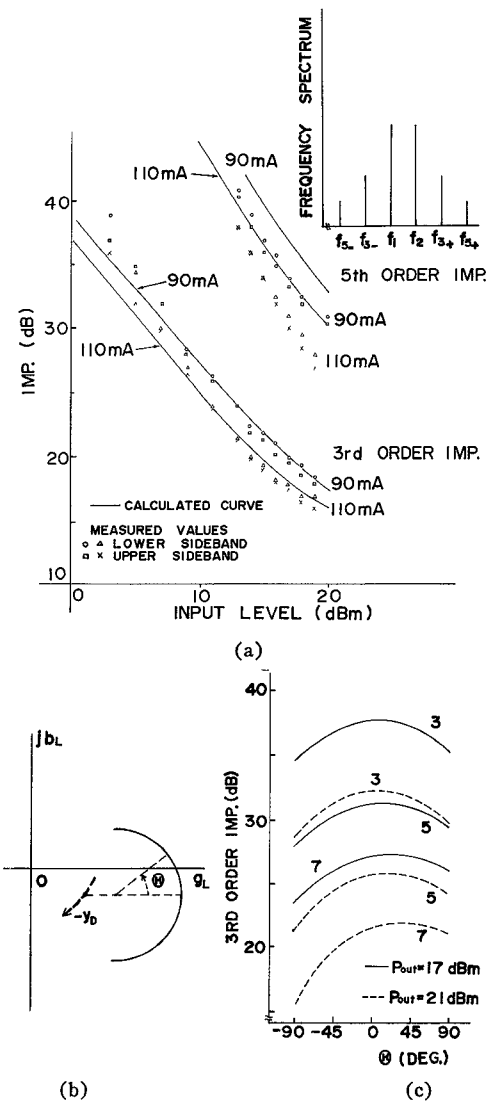

Fig. 4. (a) Measured and calculated values of the third- and fifth-order IMP's of the IMPATT amplifier. f_1, f_2—signal frequencies; f_{3+}, f_{3-}—upper and lower sideband frequencies of third IMP; f_{5+}, f_{5-}—upper and lower sideband frequencies of fifth IMP. (b) Equal gain circle in the complex admittance plane. (c) Load admittance dependency of calculated third-order IMP. Figures show the gain of the amplifier.

two output level 17 and 21 dBm, using gain as a parameter. Roughly speaking, the positive value of Θ means that the carrier frequencies are higher than the center frequency of the amplifier and negative Θ means the inverse. The variation of IMP in the band of the amplifier can be expected as low as 6 dB from Fig. 4(c). No significant improvement can be expected by adjusting the amplifier for various RF circuit conditions. Therefore, another consideration must be done to improve the IMP.

This can be deduced from the tendency of measured electronic admittance. The electronic admittance of an IMPATT diode varies due to the change of bias current as follows: the electronic conductance increases and susceptance decreases with the increase of bias current. Then, by controlling bias current, the variation of the electronic admittance due to the variation of RF input level can be compensated for a certain degree. The bias-current dependency of the electronic admittance was already measured [see Fig. 2(b) and (c)]. Now the electronic admittance is approximated as the function of $|u|$ and bias current I_{0p}. It fits the present purpose of decreasing

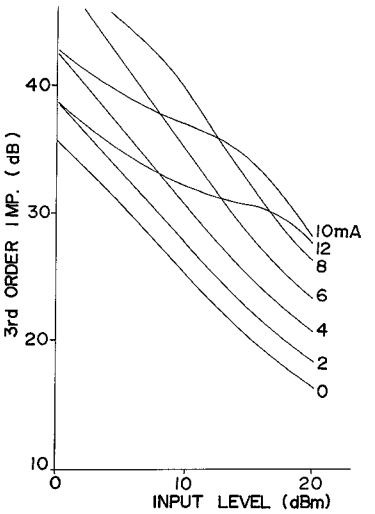

Fig. 5. Calculated third-order IMP of the IMPATT amplifier using the bias-current compensation as a parameter of the compensation current. Figures show the compensation current at input level $P_{in}=10$ dBm.

the IMP's to use the time-dependent bias current as shown in (21):

$$I_b = I_{0p} + kI_0 \cos 2pt$$
$$\bar{y}_D = \bar{y}_D(|u|, I_b) \tag{21}$$

where k is the positive constant, to show the rate of compensation current improving the IMP's. Equation (21) means to superimpose an ac current onto the dc bias current. The amplitude of this ac current is proportional to the envelope of the input RF signal voltage. The calculation of IMP's is done similarly to the way discussed previously, except using the time-dependent electronic admittance $\bar{y}_D(|u|, I_b(t_0))$. The results are shown in Fig. 5, using the parameter of compensation current. Figures in this figure show the amplitude of compensation current at the input level of 10 dBm, and the input level P_{in} means the summed power of two input signals with equal amplitude. The third-order IMP's are decreased to 40 dB down from the main spectrum at 10-dBm input level with a compensation current amplitude of 8 mA for this input level. This calculated result suggests to us that the bias-current compensation mechanism will provide a great improvement of the IMP's produced in IMPATT amplifiers. Considering the mechanisms which produce the IMP, the RF circuit dependency of the IMP is similar to that of the IMPATT amplifier without compensation. Therefore, the IMP of this compensated amplifier is also dependent on the carrier frequency location to the center frequency of the amplifier. But this dependency can be expected as rather weak. Experiments were carried out to prove this mechanism, as described in the following section.

IV. Amplifier Design and Experimental Results

In an IMPATT stable amplifier, the gain (or output level) can be smoothly changed by changing the bias current. At a constant input level, the gain increases until oscillation occurs with the increase of the bias current. This is because of the bias-current dependency of the electronic admittance $\bar{Y}_D$ of IMPATT diodes, i.e., the electronic conductance increases and susceptance decreases with the increase of the bias current, as mentioned in the previous section. Therefore, with bias current controlling according to the RF input level, much im-

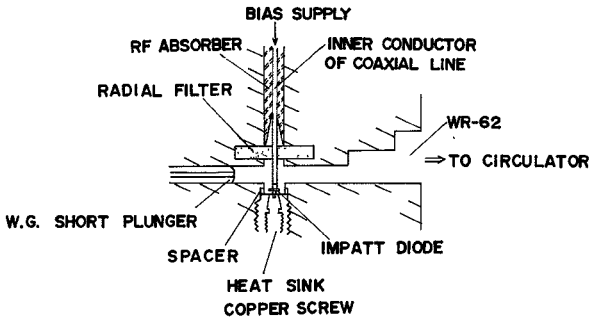

Fig. 6. Structure of *Ku*-band IMPATT-diode amplifier.

provement in linearity and amplitude-to-phase conversion characteristics of the IMPATT amplifier can be achieved, that also corresponds to the improvement in the IMP.

Fig. 6 shows the amplifier mount with a coaxial-waveguide configuration. A packaged Si-IMPATT diode is mounted on the center conductor of a coaxial line which is passed through the reduced height WR-62 waveguide. Breakdown voltage of the diode is about 62 V and typical oscillating output power is about 600 mW. The diode is held by a chuck at its end cap on the heat-sink side of the package, which provides it with good heat sinking through a large copper screw. On the opposite side of the waveguide from the diode, a radial bandstop filter (followed by a coaxial dummy load) is provided, which plays an important role in that it stabilizes the out-of-band amplifier performance, i.e., it restrains any oscillations.

Fig. 7(a) and (b) shows typical characteristics of output power P_{out} and phase shift $\Delta\phi$ (phase difference between the input and output signal) versus input signal level of 13-GHz IMPATT amplifiers with the small-signal gains of 8.6 and 4.6 dB, respectively, as a parameter of bias current I_{0p}. These two amplifiers were connected in cascade to realize a 2-stage amplifier with a total gain of 11 dB at 10-dBm input level. The first-stage amplifier has a 1-dB gain compression output level of 17.6-dBm and 1-dB down bandwidth of about 270 MHz at 10-dBm input level. The second-stage amplifier was adjusted to provide a 1-dB gain compression output level of 23.6-dBm and 1-dB down bandwidth of about 500 MHz at 10-dBm input level. Typical operating current I_{0p} and voltage V_{0p} of these amplifiers were 100 mA and 74 V, respectively. Measured third-order IMP's produced in these amplifiers are represented by the solid lines with a notation of "without-compensation" in Figs. 9(a) and (b), corresponding to the operating conditions shown in Fig. 7(a) and (b), respectively. The input level in these figures is the sum of the input powers of two equal amplitude signals f_1 and f_2 ($\Delta f = f_1 \sim f_2 = 1$ MHz). Typical third IMP values of these amplifiers are 20 dB$\sim$28 dB at the desired input level for each stage amplifier. These values of IMP are too poor for AM transmission systems use.

The diode bias-current compensation technique mentioned above was applied to these amplifiers to improve the nonlinear distortion. A basic block diagram of the bias-current compensation circuit for 2-stage amplifier is shown in Fig. 8. A very small amount of power of both input signals (f_1 and f_2) is taken out through a directional coupler and the envelope of the two-signal waveforms is detected by a diode detector. Then the detected signal is amplified by transistor amplifiers with proper gains to give optimum compensating bias currents which are superimposed on the fixed bias-current of IMPATT diodes. The output impedance of these tran-

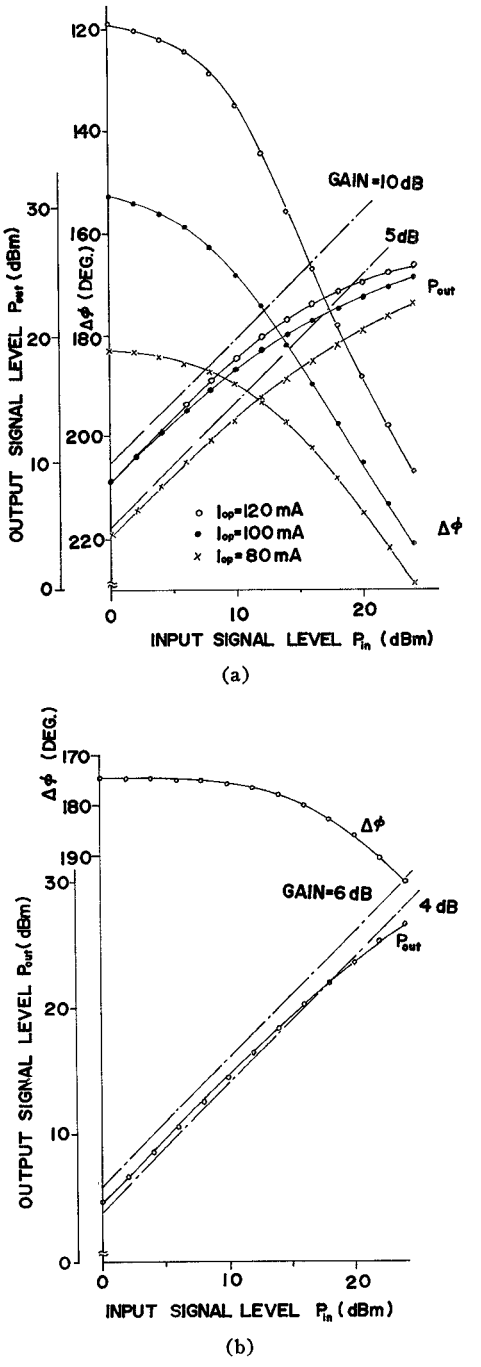

Fig. 7. (a) Typical characteristics of output power P_{out} and phase shift ϕ versus input signal level of a 13-GHz single-stage IMPATT amplifier with a small-signal gain of 8.6 dB. (b) Typical characteristics of output power P_{out} and phase shift ϕ versus input signal level P_{in} of a 13-GHz single-stage IMPATT amplifier with a small-signal gain of 4.6 dB (I_{0p}=100 mA).

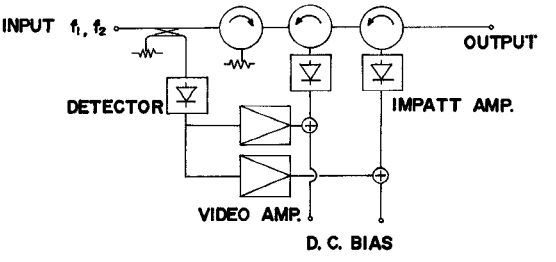

Fig. 8. Basic block diagram of the bias-current compensation circuit applied to the 2-stage IMPATT amplifier.

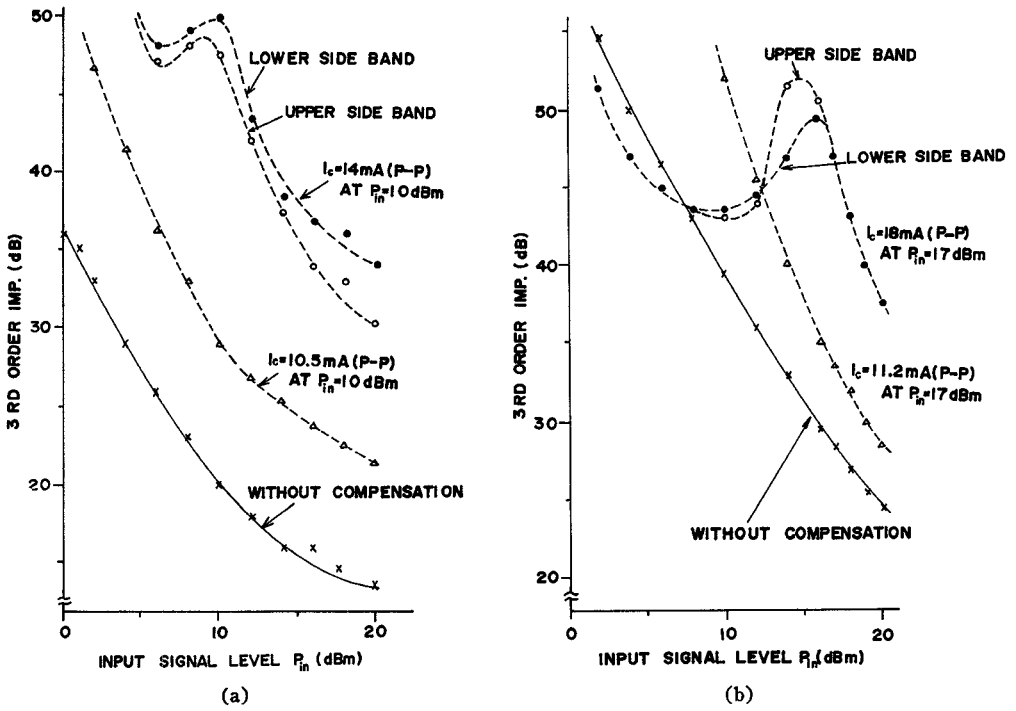

Fig. 9. (a) Third-order IMP of the single-stage amplifier with small-signal gain of 8.6 dB versus input signal level (sum of the equal amplitude two signals) as a parameter of compensation current Ic. (b) Third-order IMP of the single-stage amplifier with small-signal gain of 4.6 dB versus input signal level (sum of the equal amplitude two signals) as a parameter of compensation current Ic.

sistor amplifiers is high enough so that the impedance of bias circuits seen from IMPATT diodes is also high enough. These high-impedance bias circuits give good noise performances of the IMPATT amplifiers [5]. These transistor amplifiers have nearly constant gain in the frequency range from about 100 kHz to 20 MHz. So, present IMPATT amplifiers can be applied to the AM transmission system whose modulation frequencies are within the band of the video amplifiers.

Experimental results involving this bias-current compensation being applied to the amplifier are shown in Fig. 9(a) and (b), corresponding to the first- and second-stage amplifier, respectively, as a parameter of the compensation current. In this experiment, the gain of each transistor amplifier in the bias-current compensation circuit was adjusted to supply an optimum compensation current to the first and second amplifier at the input levels of 10 and 17 dBm, respectively. At those input levels, a third IMP of about 47 dB was obtained with the optimum compensation current of 14 and 18 mA, respectively, and more than 40 dB was guaranteed within the input level up to those values.

In Fig. 9(a) and (b), upper and lower sideband of the third IMP were almost the same, in the case of a small compensation current and without compensation.

In these experiments, input signal frequencies are $f_1 = 13.258$ GHz and $f_2 = 13.259$ GHz. The compensation current was measured at the dc bias terminal of the IMPATT diode (output terminal of the video frequency amplifier in the compensation circuit and represented by the peak-to-peak value of the detected current envelope of the 1-MHz beat frequency). If the conversion efficiency of the detector and the gain of the video frequency amplifier are kept constant, the compensation current decreases according to the decrease of the input signal level of the IMPATT amplifier. This fact limits the dynamic range of the effective compensation for a wide range of input level.

Resultant third-order IMP's produced in the 2-stage amplifier are shown in Fig. 10. Linearity characteristics with respect to the two input signals ($\Delta f = f_1 \sim f_2 = 1$ MHz) were also measured. With the bias-current compensation, 1-dB compression output level of the 2-stage amplifier increases to 21.8 dBm, which is about 2 dB larger than that of the amplifier without compensation. In Fig. 10 are also shown the compensation currents for each stage amplifier versus input level. The third-order IMP's are more than 40 dB within the input level up to 12 dBm, where the amplifier can deliver an output power of 23 dBm. The fifth-order IMP's are also more than 40 dB.

Typical examples of the output frequency spectrum of the 2-stage amplifier with an input level of 10 dBm are shown in Fig. 11(a) and Fig. 12(a) without and with bias-current compensation, respectively. The compensation current for each stage amplifier was adjusted to provide the third and fifth IMP's of more than 40 dB. The voltage waveforms (envelopes) of the output signals from the amplifier were investigated using a sampling oscilloscope. The results are shown in Fig. 11(b) and (c) for the input levels of 10 and 20 dBm in case of no compensation. Also, in Fig. 12(b) and (c) is shown the envelopes for the same input levels in case of with compensation. The improvement in the IMP's can be clearly understood from these refined waveforms resulting from the compensation being used. Finally, the IMP's caused by these compensated amplifiers are influenced by the change of the ambient temperature. Main factors causing the temperature dependency of IMP's are the variation of the follow-

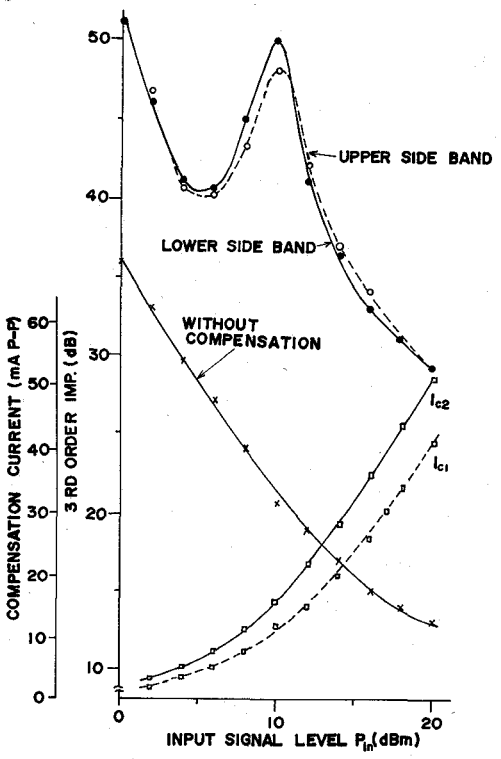

Fig. 10. Third-order IMP and compensation current of the 2-stage amplifier versus input signal level (sum of the equal amplitude two signals).

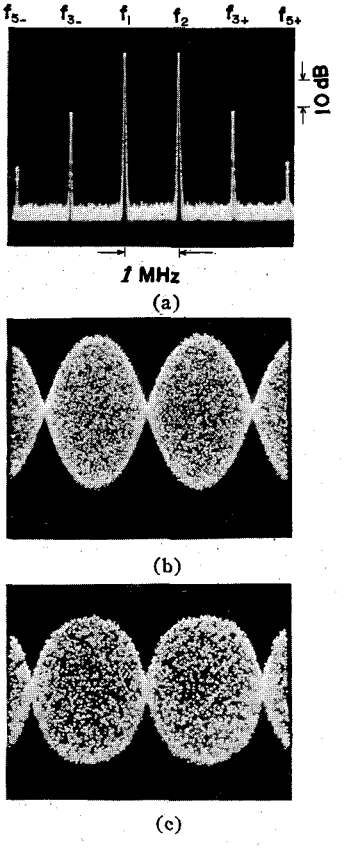

Fig. 11. Frequency spectrum and voltage waveforms of output signals of the 2-stage amplifier without bias-current compensation. (a) Frequency spectrum at $P_{in}=10$ dBm. Horizontal scale—0.5 MHz/div; vertical scale—10 dB/div. (b) Voltage waveform at $P_{in}=10$ dBm. Horizontal scale—0.25 μs/div. (c) Voltage waveform at $P_{in}=20$ dBm. Horizontal scale—0.25 μs/div.

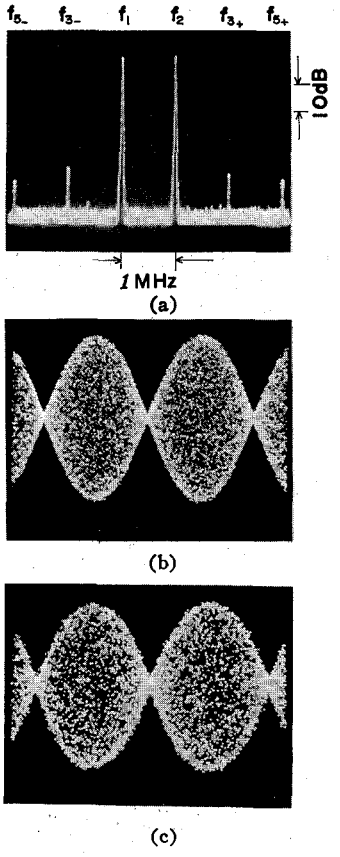

Fig. 12. Frequency spectrum and voltage waveforms of output signals of the 2-stage amplifier with bias-current compensation. (a) Frequency spectrum at $P_{in}=10$ dBm. Horizontal scale—0.5 MHz/div; vertical scale—10 dB/div. (b) Voltage waveform at $P_{in}=10$ dBm. Horizontal scale—0.25 μs/div. (c) Voltage waveform at $P_{in}=20$ dBm. Horizontal scale—0.25 μs/div.

ing parameters by the change of ambient temperature: 1) the gain of the IMPATT amplifiers and 2) the conversion ratio from the RF signal to the video signal (envelope) of the detectors. The resultant IMP's caused by these compensated amplifiers were in the range better than 37 dB within the temperature range from −10 to 40°C.

V. Conclusion

A bias-current compensation technique is described, which is one of the practical methods to reduce the nonlinear distortion produced in the stable IMPATT amplifier. This technique has been successfully applied to a 13-GHz 2-stage IMPATT amplifier in the transmitter of a TV transmission microwave system. This technique will provide further application of IMPATT-diode amplifiers to the amplitude modulation transmission systems.

Acknowledgment

The authors wish to thank Dr. S. Kojima, Managing Director, F. Iwai, Assistant Director, both of Fujitsu Laboratories Ltd., and S. Kaneko, Manager of the Radio Engineering Department, H. Nishiyama, Chief Engineer of the Radio Engineering Department, and T. Horiba, Chief Engineer of the Semiconductor Engineering Department, all of Fujitsu Ltd., for their encouragement during this study. They also wish to thank N. Kanda, of the Radio Engineering Department, Fujitsu Ltd., for his helpful discussion.

References

[1] S. Nagano and H. Kondo, "Highly stabilized half-watt IMPATT oscillator," *IEEE Trans. Microwave Theory Tech. (Special Issue on Microwave Circuit Aspects of Avalanche-Diode and Transferred Electron Devices)*, vol. MTT-18, pp. 885–890, Nov. 1970.

[2] H. Komizo *et al.*, "K-band high power single-tuned IMPATT oscillator stabilized by hybrid-coupled cavities," *1972 G-MTT Dig. Tech. Papers*, pp. 176–178.

[3] H. J. Thaler, G. Ulrich, and G. Weidmann, "Noise in IMPATT diode amplifiers and oscillators," *IEEE Trans. Microwave Theory Tech.*, vol. MTT-19, pp. 692–705, Aug. 1971.

[4] I. Tatsuguchi, N. R. Dietrich, and C. B. Swan, "Power-noise characterization of phase-locked IMPATT oscillators," *IEEE J. Solid-State Circuits (Special Issue on Solid-State Microwave Circuits)*, vol. SC-7, pp. 2–10, Feb. 1972.

[5] H. Komizo, Y. Ito, H. Ashida, and M. Shinoda, "A 0.5-W CW IMPATT diode amplifier for high-capacity 11-GHz FM radio-relay equipment," *IEEE J. Solid-State Circuits (Special Issue on Microwave Integrated Circuits)*, vol. SC-8, pp. 14–20, Feb. 1973.

[6] F. Ivanek, "Single-sideband amplitude modulation in microwave transmission systems," *Microwave J.*, pp. 27–36, Apr. 1972.

[7] R. J. Trew *et al.*, "Intermodulation characteristics of X-band IMPATT amplifiers," *1972 G-MTT Dig. Tech. Papers*, pp. 182–184.

[8] H. Seidel, "A feedforward experiment applied to an L-4 carrier system amplifier," *IEEE Trans. Commun. Technol.*, vol. COM-19, pp. 320–325, June 1971.

Analysis of Phase Characteristics as a Function of Ambient Temperature of IMPATT Amplifiers

LARRY I. YARRINGTON AND PHILLIP W. HAWKINS

***Abstract*—Experimental data on phase characteristics as a function of ambient temperatures for GaAs IMPATT amplifiers are presented. An evaluation is given to show the impact of ambient temperature on an amplifier design used in phased-array radars.**

Introduction

IT HAS BECOME apparent that, to avoid network feed loss in some phased-array applications, individual amplifiers for each antenna element would be desirable. However, this requires amplifiers of small size, low cost, and high reliability which, at the same time, have characteristics that are well understood. It is especially important with IMPATT-diode amplifiers used in airborne environments, since the RF phase in these devices is quite susceptible to changes in ambient temperature.

The purpose of this paper is to provide empirical data on solid-state amplifiers which have been designed for phase-array applications.

Experiment

The objective of the experiment was to precisely measure the phase of the forward transmission coefficient of the avalanche diode amplifier (ADA) while monitoring the ambient temperature of the diode. A Hewlett-Packard network analyzer was used for measuring the transmission coefficient. The normal equipment configuration had to be modified in order to supply the desired input power to the amplifier. Fig. 1 depicts the setup employed. The system is basically a standard microwave bridge. The technique is used with the network analyzer in the reference arm, but which bypasses part of the test arm of the analyzer.

During testing, the amplifier was mounted on a water-bath heat sink. The baseplate temperature of the amplifier was controlled by varying the temperature of the water into the heat sink. The cooling equipment used permitted continuous water temperature regulation from 0 to 70°C, which resulted in measured temperatures at the diode mount of 11.7–69.7°C. Ambient temperature of the diode was monitored by a thermocouple attached to the diode mount. The amplifier/heat-sink assembly was mounted in a box to isolate the diodes from possible air drafts.

The amplifiers tested were GaAs ADA's made under Air Force contract F33615-69-C-1830. These 4-stage circulator-coupled reflection amplifiers were designed in alumina-substrate microstrip circuits with each diode individually biased and tuned. The nominal output power from each amplifier was 1 W from 9.0 to 9.6 GHz with a gain of 17 dB.

All operating points for these tests were chosen to be within the amplifier design criteria. Input power was selected as +8.5 dBm. The oscillator was set to sweep from 9.0 to 9.6 GHz. Table I lists the pertinent device parameters. Fig. 2 is a photograph of the amplifier.

Five of these amplifiers were to be tested but one of them failed in test. Of the four remaining amplifiers all showed the same experimental results in relative phase shift versus change in ambient temperature.

Phase measurements on the amplifier were taken every 9°C over the temperature range with zero reference phase arbitrarily taken near room temperature (26.3°C) Thermal expansion of the microstrip circuit and circulators were expected to contribute to the amplifier phase shift. To isolate this factor the circulator strip was removed from one of the amplifiers and phase measurements taken over the temperature range 26.3–71.1°C. No practical method was avail-

Manuscript received February 5, 1973; revised July 9, 1973.

L. I. Yarrington is with the Air Force Avionics Laboratory, Wright-Patterson AFB, Ohio.

P. W. Hawkins was with the Air Force Institute of Technology, Wright-Patterson AFB, Ohio. He is now with the Ocean Engineering Division, U. S. Coast Guard Headquarters, 400 7th St. SW, Washington, D. C. 20590.